ARTICLE

^Received 00th January 20xx,
Accepted 00th January 20xx

DOI: 10.1039/x0xx00000x

How does the composition of a PAH influence its microsolvation? A rotational spectroscopy study of the phenanthrene-water and phenanthridine-water clusters

Donatella Loru,*[a] Amanda L. Steber,[a] Pablo Pinacho,[a] Sébastien Gruet,[a] Berhane Temelso,[b] Anouk M. Rijs,[c] Cristóbal Pérez [a] and Melanie Schnell [a,d]

We report on the noncovalent intermolecular interactions established between the polycyclic aromatic hydrocarbons phenanthrene and phenanthridine with water. Such noncovalent interactions involving extended aromatic systems and water molecules are ubiquitous in a variety of chemical and biological systems. Our study provides spectroscopic results on simple model systems to understand the impact that an extended aromatic surface and the presence of a heteroatom have on the nature of the noncovalent interactions established with the solvent. Microhydrated phenanthrene and phenanthridine clusters with up to three water molecules have been observed and unambiguously characterised by means of broadband rotational spectroscopy and quantum chemical calculations. The presence of a nitrogen atom in the backbone of phenanthridine remarkably affects the geometries of the water clusters and the interaction networks at play, with O–H···N and C–H···O interactions becoming preferred in the phenanthridine-water clusters over the O–H···π interactions seen in the phenanthrene-water clusters. The presence of this heteroatom induces nuclear quadrupole coupling, which was used to understand the cooperativity effects found with increasing cluster size. Our results provide important insight to draw a more complete picture of the noncovalent interactions involving solvent molecules and aromatic systems larger than benzene, and they can be significant to enhance our understanding of the aromatic-polar interactions at play in a myriad of chemical and biological contexts.

Introduction

Noncovalent intermolecular interactions involving aromatic rings and water, i.e., π···H–O and C–H···O interactions, are considered to be the driving force in many biological and chemical processes.[1] In particular, noncovalent interactions occurring between aromatic carbonaceous based materials, such as polycyclic aromatic hydrocarbons (PAHs), and water molecules play an important role in many different areas, ranging from biomolecular recognition to astrochemistry. In the context of astrochemistry, for example, the detection of PAHs in cosmic ices suggests that they might behave as nucleation sites during the formation of interstellar ice mantles,[2] in which PAHs are embedded and influence the chemistry.

Laboratory studies have demonstrated that, when embedded in water dominated ices and in the presence of UV light, PAHs can undergo photochemical processes to form more complex organic molecules. Most of these species are of biogenic interest, such as quinones, ethers, and aromatic alcohols.[3,4] These photoinduced mechanisms have not yet been understood. Even so, such processes are likely to be influenced by the morphology of the interstellar ices, which is in turn expected to be influenced by the intermolecular interactions established with the PAH. Therefore, an accurate knowledge of the fundamental intermolecular interactions can be important to understand the formation of interstellar ice grains and the chemistry occurring in these environments. Detailed knowledge of the geometries of (micro)hydrated PAH clusters can also be of interest for astrochemical modelling.

Despite their importance, there is a lack of experimental studies aimed at the investigation of these fundamental interactions in aromatic systems larger than benzene and featuring different structural topologies. As the structure of

[a] Deutsches Elektronen-Synchrotron (DESY), Notkestraße 85, 22607 Hamburg, Germany.
[b] Division of Information Technology, College of Charleston, Charleston, SC 29424, USA
[c] Division of BioAnalytical Chemistry, AIMMS Amsterdam Institute of Molecular and Life Sciences, Vrije Universiteit Amsterdam, De Boelelaan 1108, 1081 HV Amsterdam, The Netherlands.
[d] Institute of Physical Chemistry, Christian-Albrechts-Universität zu Kiel, Max-Eyth-Straße 1, 24118 Kiel, Germany.
* Corresponding author. E-mail: donatella.loru@desy.de
Electronic Supplementary Information (ESI) available: [details of any supplementary information available should be included here]. See DOI: 10.1039/x0xx00000x

the substrate can have an impact on the nature and strength of its interactions with the surrounding molecules, it is important that these knowledge gaps are filled. Only recently, laboratory studies have focused on the initial steps of water aggregation in the presence of larger PAHs. For example, the microhydrated complexes of the PAH acenaphthene (Ace) have been extensively investigated in the gas phase using cutting-edge spectroscopic techniques, such as chirped pulse Fourier transform microwave (CP-FTMW) spectroscopy and IR-UV ion dip spectroscopy coupled with a molecular beam.[5,6] Water complexes with the smallest chiral PAH helicene and with the bowl-shaped corannulene have also been characterised using CP-FTMW spectroscopy.[7,8] In the cationic form, the hydrated clusters of naphthalene$^+$ have been studied by infrared photodissociation (IRPD) spectroscopy.[9] These studies have all provided important information regarding the structures and the intermolecular interactions in these clusters. For example, the spectroscopic investigation of the hydrated clusters of the PAH acenaphthene revealed that in such complexes the interactions within the water molecules are dominant with the water retaining most of the structural characteristics of the pure water cluster.

The study of the hydrated clusters of naphthalene$^+$ cation showed the impact that an extended aromatic surface has on the hydrogen bond interactions established between the water molecules and the substrate. A comparison between the water complex of naphthalene$^+$ with those of benzene$^+$ revealed interesting differences. Although the positively charged density is more localised in the benzene$^+$ and the interaction with the water was expected to be stronger than in the naphthalene$^+$, the presence of fused aromatic rings in the latter accounts for a molecular orbital interaction making the hydrogen bonds (HBs) stronger in naphthalene$^+$ than in benzene$^+$.

A more comprehensive picture of the intermolecular interactions that a PAH molecule establishes with the surrounding water molecules can be gained by extending the investigation to PAHs of different shape, size, and degree of aromaticity than those already studied, as well as substituted PAHs, i.e., PAHs incorporating one or more heteroatoms into the carbon skeleton.

In the present work, we have used broadband CP-FTMW spectroscopy to investigate the first steps in microsolvation of phenanthrene (Phe) and phenanthridine (Pan) (Figure 1). These two molecules have closely related structures since both feature three fused fully aromatic six-membered rings, which only differ by one nitrogen atom. The outstanding sensitivity of the technique allowed for the determination of accurate experimental structures of these hydrated complexes. We observed how the presence of a nitrogen atom and a planar geometry of the substrate drastically influences the water aggregation motifs and the strength of the hydrogen-bond network at play on a large aromatic surface. A thorough comparison with the previously studied hydrated clusters of the PAH Ace is provided. Differently from Phe, Ace is not fully aromatic, but has dangling C–H bonds that can be used as an anchor point for the water molecules. An exhaustive analysis of the intermolecular interactions stabilising the hydrated clusters of the two molecules highlights the crucial role that the composition of the PAH plays in determining the interaction network at play in such systems.

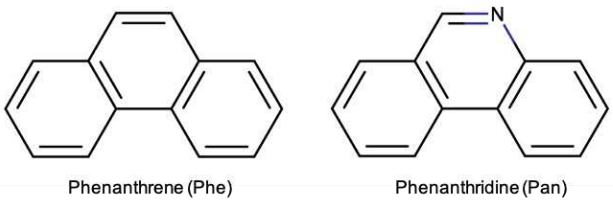

Figure 1 Chemical structures of phenanthrene (left) and phenanthridine (right).

Experimental and computational methods

The spectroscopic measurements were performed using the CP-FTMW spectrometer COMPACT, of which a detailed description has been previously reported.[10,11] The samples of Phe ($C_{14}H_{10}$, 98% purity) and Pan ($C_{13}H_9N$, 98% purity) were purchased from Sigma Aldrich and used without any further purification. Both molecules appear as a white/yellowish powder with tabulated melting points of 101 °C and 107 °C for Phe and Pan, respectively. To transfer the molecules into the gas phase, the sample was placed into a heatable reservoir situated at the orifice of a modified pulsed valve (Parker General Valve, Series 9). A temperature of ca. 130 °C was found to be optimal to obtain a sufficient vapor pressure for both molecules. Hydrated clusters were formed by connecting a reservoir containing water external to the vacuum chamber. The supersonic expansion was created by flowing neon, used as a carrier gas, at a backing pressure of ca. 3.5 bar over the two reservoirs.

Upon supersonic expansion in the spectrometer chamber, the molecules were probed by a 4 μs long microwave chirped pulse spanning 2-8 GHz, which was generated by an arbitrary waveform generator. The chirped pulse was amplified by a travelling wave tube amplifier and then broadcast inside the vacuum chamber by a horn antenna. The emission signal produced by the molecular relaxation (free induction decay, FID) following microwave excitation was recorded by the receiving horn, amplified using a low noise amplifier, and subsequently digitised in the time domain by the oscilloscope. Each FID was recorded for 40 μs. The experimental spectrum in the frequency domain was obtained upon fast Fourier transformation of the signal in the time domain. The repetition rate of the experiment was set to 8 Hz; in addition, the fast frame mode of the oscilloscope was applied to all the experiments. Thus, each molecular pulse was probed by eight microwave chirped pulses, resulting in an effective repetition rate of 64 Hz.

Structural information of the clusters is extracted from the changes in the moments of inertia induced upon isotopic substitution. In this respect, experiments using an isotopically

enriched sample of $H_2{}^{18}O$ were also performed. Singly-substituted ^{18}O isotopologues of the Phe/Pan-water complexes were formed by using H_2O:$H_2{}^{18}O$ mixtures with different ratios. For instance, a 2:1 and a 3:1 H_2O:$H_2{}^{18}O$ mixture was used to generate ^{18}O monosubstituted isotopologues of the Phe/Pan-$(H_2O)_2$ and Phe/Pan-$(H_2O)_3$ clusters, respectively.

To obtain the initial fits of the experimental transition frequencies, the program PGOPHER[12] was used. Final experimental spectroscopic parameters of all the assigned species were obtained using the Watson's A- or S-reduced Hamiltonian, depending on the value of Ray's asymmetry parameter, in the I^r representation as implemented in the SPFIT/SPCAT program by Pickett.[13] The programs KRA and EVAL were used to calculate the substitution structure, r_s, while the effective structure, r_0, and the mass dependent structure, $r_m^{(1)}$, were determined using the program STRFIT. The SPFIT/SPCAT, KRA, EVAL, and STRFIT software can all be found at the PROSPE website.[14]

The spectral assignment was supported by electronic structure calculations. The equilibrium structures of the monomers of Phe and Pan were calculated using Møller Plesset perturbation theory (MP2)[15] coupled with the aug-cc-pVDZ basis set.[16] For the water clusters, a configurational sampling was performed, using a genetic algorithm approach (GA)[17] implemented in the OGOLEM[18] package on PM7[19] and HF-3c[20] potential energy surfaces implemented in MOPAC[21] and ORCA[22,23] software, respectively. The structures found to be stable minima were then further optimised at the MP2/aug-cc-pVDZ and at the B3LYP-D3BJ/def2-TZVP[24,25] levels of theory. Single point energy calculations using the MP2-F12/aug-cc-pVTZ-F12 method have been performed on the structures optimised at the MP2/aug-cc-pVDZ level of theory to remove most of the basis set superposition error (BSSE) and to get more accurate energies. Frequency calculations have been performed at the B3LYP-D3BJ/def2-TZVP and at the MP2/aug-cc-pVDZ levels of theory to verify that the predicted structures are real minima of the potential energy surface (PES). The theoretical structures, spectroscopic parameters, and relative energies of all the geometries are reported in the Supporting Information (SI).

In order to break down the different energy contributions of intermolecular interaction types as well as the overall interaction energy of the clusters, symmetry adapted perturbation theory (SAPT) calculations were performed using the PSI4 package[26] and the SAPT2+3/aug-cc-pVDZ level of theory on the MP2/aug-cc-pVDZ optimised geometries. This method is generally applied to two-body molecular systems. However, in the Phe-water clusters containing more than one water molecule, the water molecules are held together by strong O–H···O hydrogen bonds, whereas the overall complex is mainly stabilised by weaker HBs and dispersion interactions between Phe and the water moieties. As such, to carry out an SAPT analysis, the Phe-$(H_2O)_{n=1-3}$ clusters could be treated as two-body systems, where the water clusters are considered as one unit and the Phe molecule acts as the second body. Concerning the hydrated clusters of Pan, this method was not applied to its higher order hydrated clusters, since in these clusters each individual molecule is involved in stronger interactions with the substrate Pan compared to Phe. Therefore, the SAPT analysis was only performed on the Pan-H_2O complex. The noncovalent interactions were further investigated and visualized by applying the Noncovalent Interactions (NCI) method[27] using the Multiwfn program.[28] This method is based on the analysis of the derivatives of the electron density to reveal the intermolecular interactions at play in a molecular system.

A natural bond orbital analysis (NBO)[29] was also performed on the observed Pan-water clusters to calculate the change in the distribution of the electron density in the nitrogen atom upon water complexation to accompany the analysis of the ^{14}N nuclear quadrupole coupling parameters. The NBO analysis has been carried out on the structures optimised at the B3LYP-D3BJ/6-311++G(2d,p) level of theory, which are found to be comparable with those obtained at the methods previously mentioned.

Nudged elastic band calculations (NEB)[30] at the B3LYP-D3BJ/def2-TZVP level of theory have been performed to calculate the barrier for the interconversion motion between isomers 1 and 2 of the Phe-$(H_2O)_3$ cluster.

Results and discussion

Rotational spectroscopy of the Pan monomer and its water clusters

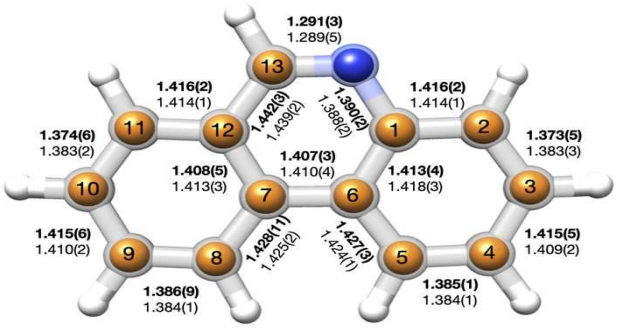

Figure 2 Comparison between the r_s and $r_m^{(1)}$ structures of Pan. The full body of the molecule represents the $r_m^{(1)}$ structure. The orange and blue spheres correspond to the carbon and nitrogen positions determined using Kraitchman's equations (r_s), respectively. The values of the r_s (bold) and $r_m^{(1)}$ (non-bold) bond lengths are given in the unit of Å.

Precise structural information on the substrate monomer is crucial to understand distortions induced in the PAH framework upon complexation with water. The structure of the monomer of Phe cannot be investigated using microwave spectroscopy, as it only has a negligible dipole moment along the *b* inertial axis ($|\mu_b|$ = 0.006 D) making Phe invisible to this technique. In Pan, the presence of the nitrogen atom in its backbone induces a substantial dipole moment ($|\mu_a|$ = 1.3 D and $|\mu_b|$= 1.8 D), thereby making this molecule suitable for a microwave spectroscopic investigation. Its experimental

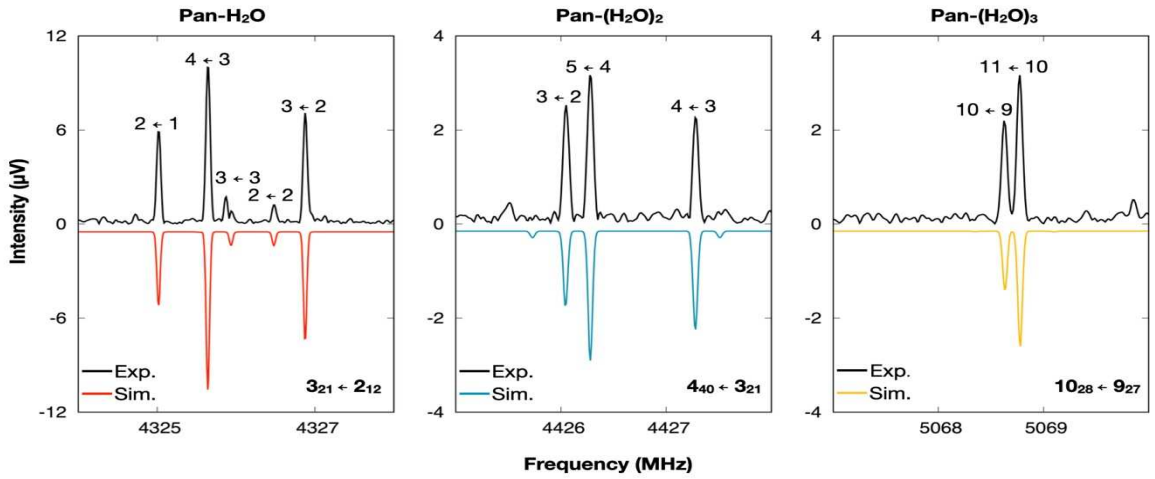

Figure 3 Sections of the broadband rotational spectrum recorded in the 2-8 GHz frequency range showing representative transitions of the Pan-H_2O (left), Pan-$(H_2O)_2$ (middle), and Pan-$(H_2O)_3$ (right) clusters. The black trace is the experimental spectrum while the coloured traces represent the simulated spectra based on the experimental rotational constants and at a rotational temperature of 2 K. The spectrum of Pan-$(H_2O)_{n=1-3}$ was recorded by averaging ~4.1M ΦΙΔσ. Τρανσιτιονσ ηαωε βεεν μαρκεδ υσινγ τηε $\vartheta_{K\alpha K\chi}$ νοτατιον (βοττομ ριγητ), ωηερε ϑ ισ τηε θυαντυμ νυμβερ ρεπρεσεντινγ τηε τοταλ ανγυλαρ μομεντυμ, ανδ K_α ανδ K_χ αρε τηε προφεχτιονσ οφ τηε ανγυλαρ μομεντυμ οντο τηε α ανδ χ σψμμετρψ αξεσ ιν τηε λιμιτινγ χασε οφ προλατε ανδ οβλατε σψμμετριχ τοπσ, ρεσπεχτιωελψ. Τηε σπεχτρα εξηιβιτ ηψπερφινε στρυχτυρε αρισινγ φρομ τηε νυχλεαρ θυαδρυπολε χουπλινγ οφ τηε ^{14}N νυχλευσ, ωηιχη ηασ βεεν λαβελλεδ φολλοωινγ τηε $\Phi \leftarrow \Phi'$ νοτατιον (τοπ τραχε).

spectrum was previously investigated between 2 GHz and 85 GHz using high resolution microwave spectroscopy by McNaughton *et al.*[31,32] In this study, spectroscopic parameters such as rotational, centrifugal, and nuclear quadrupole coupling constants were determined. However, no experimental structural data was reported. In the present work, we reinvestigated the spectrum of Pan in the 2-8 GHz frequency range. The experimental transitions that we measured for the parent species agreed with those previously published. In addition, we also observed the ^{13}C and ^{15}N singly-substituted isotopologues in natural abundance. This information allowed us to determine the structural parameters of the heavy atom skeleton. The experimental frequencies for each isotopic species were fitted using the Watson's A-reduced Hamiltonian as for the parent species. The derived spectroscopic parameters and the rotational transition frequencies for the parent species and its isotopologues are reported in Tables S1-S2 and S53-S67 of the SI. Investigation of the planar moments of inertia revealed that the P_c component remains almost unvaried upon isotopic substitution, thus indicating that the nitrogen and the carbon atoms sit in the *ab* plane (Figure S2) and the molecule is planar. The experimental rotational constants of the observed ^{13}C and ^{15}N singly-substituted isotopologues were used to determine the experimental structure of Pan. We have employed different structural determination methods, as stated in the methods section. Using the Kraitchman's equations,[33] we have determined the substitution structure, r_s, where the absolute values of the experimental coordinates of each substituted atom were determined. The signs for each coordinate were adopted from the *ab initio* structure calculated at the MP2/aug-cc-pVDZ level of theory. Least-squares procedures were also employed to determine the effective structure in the vibrational ground state, r_0, and the mass dependent structure, $r_m^{(1)}$. The latter differs from the r_0 approach as it takes into account perturbations induced by vibration-rotation contributions.[34,35] As in the case of the PAH acenaphthene,[5] the rotational constants of Pan are severely perturbed by low lying out-of-plane vibrational modes of the hydrogens (> 300 cm^{-1}).[31] This is reflected in the large deviation of the r_0 fit of 0.181 uÅ^2 and in the negative value of the inertial defect ΔI (~ -0.4 amu.Å^2). For this reason, an accurate determination of the r_0 structure was not possible, and only the r_s and $r_m^{(1)}$ structures have been taken into consideration for further discussion.

An overlay of the $r_m^{(1)}$ and the r_s structures, together with the values determined for the C–C and C–N bond distances, is depicted in Figure 2. The two structures are in excellent agreement (within their experimental uncertainties), with both methods predicting the N–C13 distance ($r_m^{(1)}$ = 1.289(5) Å and r_s = 1.291(3) Å) as the shortest distance and the C13–C12 ($r_m^{(1)}$ = 1.439(2) Å and r_s = 1.442(3) Å) as the longest. Similar values have also been obtained for the r_e structure calculated at the MP2/aug-cc-pVDZ level of theory (Table S4).

Complexation of Pan with water led to the identification of the Pan–$(H_2O)_n$ complexes, with n = 1–3 water molecules, in the rotational spectrum. The rotational spectra of the observed Pan-$(H_2O)_{n=1-3}$ clusters were obtained simultaneously from one measurement. Representative transitions of each species are displayed in Figure 3, and their experimental spectroscopic parameters are summarized in Table 1. Experimental

Table 1 Comparison between experimental and theoretical (MP2/aug-cc-pVDZ) spectroscopic constants for Pan-$(H_2O)_{n=1-3}$ complexes.

	Pan-H_2O	Pan-$(H_2O)_2$	Pan-$(H_2O)_3$

	Calc.	Exp.	Calc.	Exp.	Calc.	Exp.
A (MHz)	917.7	914.41591(24)[a]	512.9	517.04406(16)	472.2	475.70658(34)
B (MHz)	465.1	471.04386(11)	470.4	468.95668(11)	349.6	347.91926(14)
C (MHz)	308.9	311.110540(89)	245.8	246.430565(81)	202.9	203.57118(10)
Δ_J (kHz)	-	0.01791(53)	-	0.01968(82)	-	0.02792(32)
Δ_{JK} (kHz)	-	-0.1222(22)	-	0.1830(32)	-	-
Δ_K (kHz)	-	0.665(12)	-	-0.1882(45)	-	-
δ_j (kHz)	-	0.00759(29)	-	0.00814(40)	-	0.01050(18)
δ_k (kHz)	-	-	-	0.1141(14)	-	0.0351(15)
χ_{aa} (MHz)	-	-2.6107(35)	-	-2.761(32)	-	0.3453(87)
χ_{bb} (MHz)	-	-0.3110(49)	-	0.059(19)	-	-2.898(18)
χ_{cc} (MHz)	-	2.9218(49)	-	2.703(19)	-	2.552(18)
P_a (uÅ)	1086.0	1072.32376(27)	1072.5	1075.51226(39)	1433.1	1436.38331(78)
P_b (uÅ)	550.1	552.11174(27)	983.5	975.28453(39)	1057.7	1046.18325(78)
P_c (uÅ)	0.6	0.56786(27)	1.8	2.15445(39)	12.5	16.19222(78)
$\lvert\mu_a\rvert/\lvert\mu_b\rvert/\lvert\mu_c\rvert$ (D)[b]	3.9/2.0/1.3	y/y/n	3.2/0.5/0.4	y/n/n	2.3/0.6/0.6	y/n/n
# lines [c]	-	441	-	407	-	426
σ (kHz)[d]	-	6.5	-	5.8	-	6.7

[a] Standard error in parentheses in the unit of the last digit.

[b] Yes (y) or no (n) observation of *a*-, *b*-, and *c*-type transitions.

[c] Number of rotational transitions fitted.

[d] Standard deviation of the fit.

rotational transition frequencies of the observed Pan–$(H_2O)_{n=1-3}$ clusters are provided in Tables S68, S70, and S73 of the SI.

The structural assignment of the observed complexes was first achieved by a comparison of the experimental rotational constants with those predicted by *ab initio* calculations and further confirmed with the observation of their ^{18}O monosubstituted isotopologues. The observation of the latter allowed for the determination of the exact positions of the oxygen atoms of the water molecules within the cluster, which allowed for an unambiguous assignment of the observed clusters to specific molecular structures. Spectroscopic constants of the ^{18}O isotopologues are summarised in Tables S5-S7 of the SI, and they were used to determine the r_s, r_0, and $r_m^{(1)}$ experimental structures of the observed clusters. A comparison of the determined structural parameters for all structure determination methods employed is provided in Tables S8-S12 of the SI. An improvement of the least-squares fits was observed when including correction terms accounting for molecular vibrations, particularly in the case of Pan-$(H_2O)_2$. For this reason, the following discussion will only be based on the structures obtained at the $r_m^{(1)}$ method.

In Figure 4, the $r_m^{(1)}$ structures are displayed along with the experimental and theoretical O···N and O···O distances. The identified complexes exhibit a quasi-planar geometry, which was also confirmed by the almost unchanged values of the P_c component of the planar moment of inertia upon isotopic substitution (Tables S5-S7). In all clusters, the water complexes to Pan by forming a primary O–H···N hydrogen bond. As is evident from the NCI analysis in Figure 4, C–H···O secondary interactions are also established between the oxygen free lone pairs and the nearest aromatic hydrogen atoms, and they further anchor the water molecules to Pan. There are no O–H···π interactions formed between the water and the aromatic π cloud of Pan in any of the experimentally observed complexes. Instead, the nitrogen atom guides the water towards a linear aggregation motif along the outer perimeter of Pan.

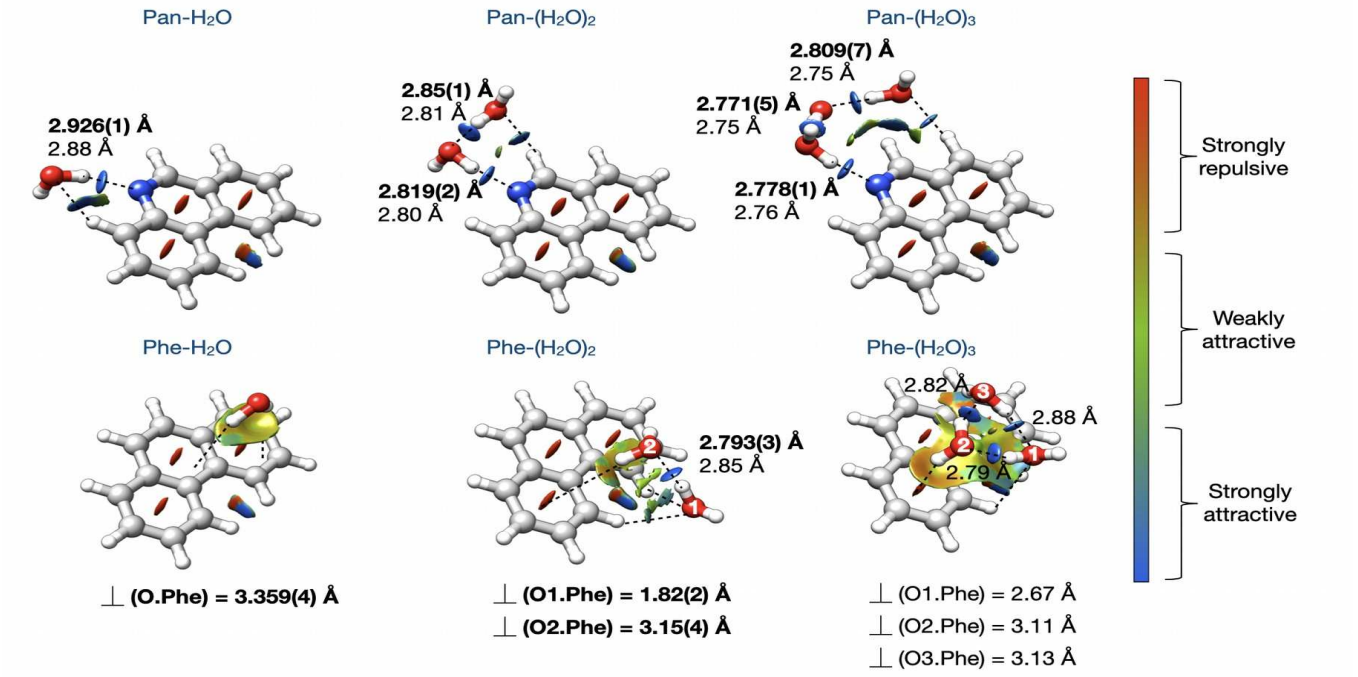

Figure 4 Structures of the observed complexes of Pan-$(H_2O)_{n=1-3}$ (top) and Phe-$(H_2O)_{n=1-3}$ (bottom). The $r_m^{(1)}$ structures are illustrated for Pan-$(H_2O)_{n=1-3}$ and Phe-$(H_2O)_{n=1-2}$. The structure of Phe-$(H_2O)_3$ corresponds to the *ab initio* structure calculated at the MP2/aug-cc-pVDZ level of theory. The structure of the Phe-H_2O complex was obtained from an average of the four sets of rotational constants obtained for each of the four tunnelling states (see text). The relevant experimental O···O and O···N distances (bold) are reported and compared with those predicted from *ab initio* calculations at the MP2/aug-cc-pVDZ level of theory (non-bold). For Phe-$(H_2O)_{n=1-2}$, the experimental perpendicular distances between the oxygen atom of each water molecule and the Phe plane ⊥ (O.Phe) are also reported. The distances for Phe-$(H_2O)_3$ are from *ab initio* calculations. The NCI isosurfaces marking the location and strength of the noncovalent interactions are plotted. The relevant O–H···O/ O–H···N, C–H···O, and C–H···π ιντεραχτιονσ αρε ηιγηλιγητεδ ωιτη βλαχκ δασηεδ λινεσ.

Calculations performed using the MP2/aug-cc-pVDZ method predict a μ_c component of the dipole moment (1.3 D) in the Pan-H_2O cluster, indicating that the free hydrogen of the water molecule is out of the *ab* plane. However, we did not observe any *c*-type transitions in the experimental spectrum, indicating that the free hydrogen atom of the water is likely tunnelling between an up and down configuration. The time scale of this motion can be assumed to be too fast to be resolved by rotational spectroscopy. As a consequence, the observed structure corresponds to an average structure with the water's free hydrogen atom lying in the Pan plane.

For the Pan-$(H_2O)_3$ cluster, MP2/cc-aug-pVDZ calculations predict a complex showing a cyclic water trimer sitting over the aromatic surface of Pan to be energetically virtually degenerate with the experimentally observed one where the water assumes a linear motif (Figure S9). Note that experimentally we only observed one conformer of the Pan-$(H_2O)_3$ cluster, with a linear water arrangement. The MP2 method tends to overestimate dispersion interactions,[36] and this over-stabilisation is overcome for the MP2-F12/aug-cc-pVTZ-F12//MP2/aug-cc-pVDZ level of theory. Indeed, this method removes the degeneracy between the two complexes, and the cyclic motif of the water cluster becomes 7.7 kJ/mol higher in energy than the linear one, in agreement with our experimental observations. The non-degeneracy between the linear and cyclic motif of the water cluster was further confirmed by calculations performed at the B3LYP-D3BJ/def2-TZVP level of theory, which also predict the complex where the water cluster assumes a linear geometry as the global minimum and determines the one in which the water molecules arrange in a cyclic motif to be 7.6 kJ/mol higher in energy than the linear one (Table S14). These results confirm the overestimation of the dispersion forces by the MP2 method and validates the need to use more advanced *ab initio* methods such as MP2-F12 and the need for more structure-sensitive experiments, especially for molecular systems in which dispersion interactions are important.

A closer look at the structures of the complexes reported in Figure 4 reveals a progressive shortening of the O···N and O···O distances as the number of water molecules increases. We see, for example, that Pan-H_2O has an O···N experimental distance of 2.926(1) Å, whereas it decreases to 2.819(2) Å and 2.778(1) Å in Pan-$(H_2O)_2$ and Pan-$(H_2O)_3$, respectively. This effect is the result of both σ- and π-bond cooperativity, where

the latter is also known as Resonance Assisted Hydrogen Bonding (RAHB).[37,38] Both effects are associated with complexes in which molecules act simultaneously as a hydrogen donor and acceptor. The σ-cooperativity is observed in molecular systems in which functional groups form chains or cycles of hydrogen bonds, whereas the RAHB refers to the phenomenon in which the hydrogen bond network involves molecules having multiple conjugated π-bonds. These effects have been already observed in the gas phase in a number of water complexes, such as the formamide-water,[39] the hydantoin-water,[40] the 2-azetidinone-water,[41] and the ethyl carbamate-water complexes.[42]

In the case of Pan, complexation with water modifies the electronic environment at the quadrupolar nucleus ^{14}N with I(^{14}N) = 1, thereby affecting the coupling between the nuclear quadrupole moment and the electric field generated by the non-homogeneous distribution of electrons in the *p* orbitals of the valence shell of the ^{14}N atom, $(U_p)_i$ (i = x, y, or z*)*. This effect is revealed by the change in the values of the nuclear quadrupole coupling constants as water molecules are added to the system (Table 1).

In general, the experimental diagonal elements of the nuclear quadrupole coupling tensor (χ_{aa}, χ_{bb}, and χ_{cc}) in the principal axis system can be associated with the constants in the nuclear quadrupole nucleus tensor (χ_{xx}, χ_{yy} and, χ_{zz}) via its diagonalization. This is possible only if the complete tensor is determined, which was not the case in our experiment. However, in the case of Pan and its hydrated clusters, provided the planarity of the geometries, one of the experimental nuclear quadrupole coupling constants can be approximated with one of the constants in the traceless tensor. We have chosen to approximate χ_{cc} to χ_{zz} since the $2p_z$ orbital is perpendicular to the molecular plane, and it is involved in the resonance process responsible for the progressive increase of the polarisation at the nitrogen atom as the degree of solvation increases. The relationship linking the unbalanced electronic charge $(U_p)_z$ and χ_{zz} is given by the following equation:

$$\chi_{zz}/eQq_{210} = -¿¿$$

where eQq_{210} represents the electric field associated with a 2*p* electron in an isolated atom (-10.86(11) MHz for a ^{14}N atom).[43] $(U_p)_z$ can assume both positive and negative values corresponding to an electron deficit or excess along the *z* axis, respectively.

In Figure 5, the experimental values of χ_{cc}/eQq210 and those of $(U_p)_z$, which have been obtained from a natural bond orbital (NBO) analysis,[29] are plotted for the monomer of Pan and its observed water clusters. A linear increase for both χ_{cc} and $(U_p)_z$ upon water complexation can be observed, which reflects the changing polarization at the nitrogen nucleus. This corroborates the shortening observed in the O···N and O···O distances in the Pan-water complexes and highlights the possibility to use the nuclear quadrupole coupling constants as a way to gauge these effects,[43] thereby showing how cooperative effects can be monitored also in molecular systems for which experimental structural information is not available.

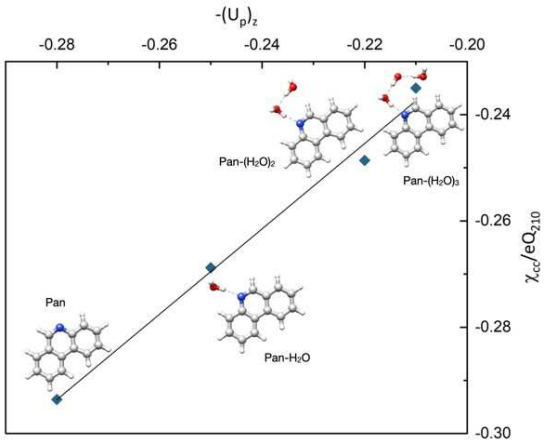

Figure 2 Correlation between the experimental values of χ_{cc}/eQq$_{210}$ and -$(U_p)_z$. The values of $(U_p)_z$ have been obtained from a natural bond orbital (NBO) analysis, those of χ_{cc} from a fit of the experimental frequencies (Table 1).

Rotational spectroscopy of the Phe-$(H_2O)_{n=1-3}$ clusters

While Phe has a negligibly small dipole moment, its complexation with water creates a permanent dipole moment enabling the observation of the experimental microwave spectra of its clusters with up to three water molecules. Representative transitions of each assigned species are shown in Figure 6, and the experimental spectroscopic parameters are provided in Table 2. In the experimental spectrum, the rotational transitions belonging to the monohydrated cluster of Phe show a characteristic quartet splitting, as can be seen in the left panel of Figure 6. This characteristic fine structure arises from two concerted tunnelling motions of the water: the internal rotation around its C_2 symmetry axis, exchanging the two equivalent hydrogen atoms, and a second large amplitude motion in which the water moves between two equivalent geometries of the cluster. These complex internal dynamics have been extensively investigated, and more detailed information can be found in a dedicated manuscript. For the sake of clarity, the structure of Phe-H_2O discussed in the rest of the depictions is an average structure of the four tunnelling states.

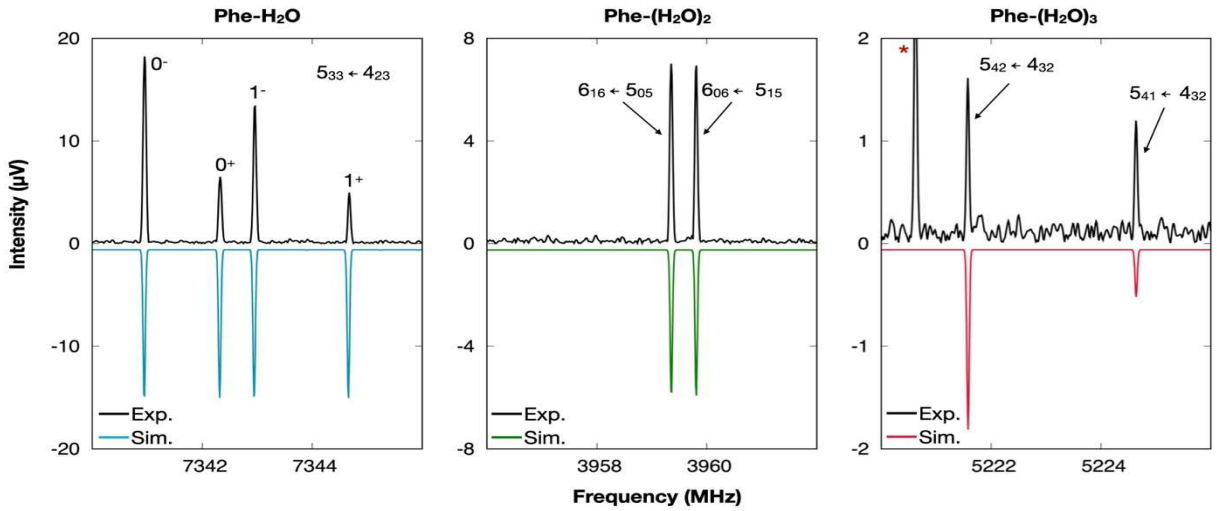

Figure 6 Sections of the experimental broadband spectrum showing representative transitions of the Phe-H_2O, Phe-$(H_2O)_2$, and Phe-$(H_2O)_3$ clusters. In each panel, the black trace represents the experimental spectrum, whereas the coloured trace represents the simulated spectra based on the experimental rotational constants and using a rotational temperature of 2 K. The overall experimental spectrum was recorded in the 2-8 GHz frequency range by averaging together 5.9 M FIDs. The splitting observed in the Phe-H_2O can be seen in the left panel. The intensities in the simulated spectrum do not take into account the spin statistics due to the exchange of the two hydrogen atoms and are set to be equal. The labelling of the four tunnelling states is also given, where 0 and 1 and + and – indicate the tunnelling states generated by the large amplitude motion and the internal rotation of the water, respectively.

Singly-substituted ^{18}O isotopologues were also assigned for the Phe-$(H_2O)_{n=1-2}$ complexes. In the case of the Phe-$(H_2O)_3$ complex, the signal-to-noise ratio achieved in the spectrum was not sufficient for the observation of its isotopologues; therefore, its structural assignment is incomplete and solely based on a comparison between the theoretical and experimental rotational constants. The spectroscopic parameters for the observed ^{18}O isotopologues are reported in Tables S31-S32 of the SI and, together with those of the parent species, were used to calculate the r_s, r_0, and $r_m^{(1)}$ structures of Phe-H_2O and Phe-$(H_2O)_2$ complexes. The internal dynamics observed in the Phe-H_2O complex significantly perturbs its structure and, therefore, the r_0 structure could not be determined. Only the $r_m^{(1)}$ structure will be taken into consideration in our discussion. A comparison of the structural parameters obtained using the different structure determination methods is reported in Tables S33-S35 of the SI. The $r_m^{(1)}$ experimental structures of the Phe-$(H_2O)_{n=1-2}$ complexes and the *ab initio* structure of the Phe-$(H_2O)_3$ complex are displayed in Figure 4 along with the experimental and theoretical O···O interaction distances and the isosurfaces showing the noncovalent intermolecular interactions (NCI).

In the Phe-H_2O cluster shown in Figure 4, the water sits above the PAH surface at a distance of 3.359(4) Å, and it engages in a dual-aromatic binding via two O–H···π interactions with one of the peripheral rings. We analysed the distribution of the electron density in the isolated Phe and found the lateral rings to have slightly more negative electron density than the middle ring (Figure S17). Even though the water is free to migrate across the surface of Phe, this distribution leads to a slightly preferred site of interaction for the water at this edge. A closer look reveals that the water C_2 symmetry axis is tilted by ca. 16.8(1)° with respect to the *c* principal axis of Phe (Figure S12). This tilt results in an asymmetric structure where the perpendicular distances between the two water hydrogens and the Phe plane differ by 0.2 Å. A similar asymmetric arrangement of the water molecule has been previously observed in the microwave spectroscopy investigation of the benzene-water cluster,[44,45] and it has also been predicted in a theoretical study of the naphthalene-water cluster.[46]

The addition of a second water molecule causes a remarkable rearrangement of the complex, which is immediately revealed when comparing the geometries of the Phe-H_2O and Phe-$(H_2O)_2$ complexes. Unlike in the one water complex, O–H···π and C–H···O interactions are present in the latter, as shown by the NCI plots in Figure 4. The water molecule interacting with the aromatic cloud, which is referred to as W2 in Figure 4, is no longer displaced over one of the peripheral rings. Instead, to accommodate the interaction of W1 with the in-plane hydrogen atoms of Phe, W2 resides 3.15(4) Å above Phe in the region between the aromatic rings, the so-called “bay region”. In the case of W1, the water molecule does not reside directly above Phe, instead it extends beyond this bay region. W1 sits 1.82(2) Å above the plane of Phe causing the water dimer plane to be tilted by approximately 28.5(2)° with respect to the Phe surface. This contrasts with the geometry observed for the

Ace-$(H_2O)_2$ cluster,[5] where both water molecules were found to sit on a plane parallel to the one of Ace, 3.18(2) Å and 3.15(2) Å above.

Interesting differences are also observed when comparing the O···O distance in the Phe-$(H_2O)_2$ complex with the O···O distance observed for the free water dimer and the two-water complex of Ace. In the Phe-$(H_2O)_2$ complex, the experimental O···O distance (2.793(3) Å) is determined to be about 0.2 Å shorter than in bare water dimer (2.98(4) Å).[47] In the isolated water dimer, the two water molecules are not affected by any local environment and only participate in one hydrogen bond. As stated previously, secondary hydrogen bond interactions are present in Phe-$(H_2O)_2$, which increase the donor and acceptor character of the water molecules, thereby strengthening the stability of the overall hydrogen bond network and resulting in a shorter interaction distance. While these differences are apparent in the comparison between Phe-$(H_2O)_2$ and the water dimer, similar hydrogen bond networks are observed for Phe-$(H_2O)_2$ and Ace-$(H_2O)_2$ clusters. Thus, one would expect that the O···O distances would be similar between the two complexes. Indeed, the structures predicted by *ab initio* calculations at the MP2-/aug-cc-pVDZ level of theory have a similar O···O distance of 2.85 Å for both systems. While the experimental O···O distance in Ace-$(H_2O)_2$ was found to be slightly longer at 2.96(3) Å, the experimental O···O distance in the Phe-$(H_2O)_2$ complex is shorter than calculated, leading to an experimental difference between these two complexes of approximately 0.2 Å. While this seems counterintuitive, a closer look at the structures reveals two possible competing forces that could be driving this difference. In Phe, the hydrogen atoms interacting with the oxygen lone pairs are aromatic hydrogens with a larger acidic character than the out-of-plane aliphatic hydrogens of Ace. As such, they are expected to increase the donor character of the water molecule acting as a hydrogen bond donor within the water dimer in the Phe-$(H_2O)_2$ cluster. Furthermore, upon interaction with the PAH, in both Phe-$(H_2O)_2$ and Ace-$(H_2O)_2$ clusters, the water dimer rearranges itself to maximise interaction with the substrate. Therefore, the shorter O···O distance observed in the Phe-$(H_2O)_2$ complex and the longer one observed in the Ace-$(H_2O)_2$ complex reflects the influence that the structure of the substrate has on the strength of the intermolecular interactions established in a cluster.

The assignment of the observed Phe-$(H_2O)_3$ cluster to one of the geometries identified as minima of the PES was non-trivial. All the computed isomers exhibit a cyclic water trimer located over the aromatic π-cloud of phenanthrene, differing only in the respective position of the water cluster on the PAH substrate and in the directionality of the hydrogen bond network: clockwise or anticlockwise (Figure S16). Since the latter only slightly affects the stability of the clusters, in Figure 7 we only showcase the four lowest energy isomers exhibiting a clockwise motif of the HB network.

Due to their geometric similarities, a comparison between experimental and theoretical rotational constants did not allow the observed Phe-$(H_2O)_3$ complex to be unambiguously assigned to one of the calculated geometries (Table S48). However, a careful analysis of the predicted dipole moment components, the type of rotational transitions observed in the experimental rotational spectrum and their relative intensities provided more information and helped to narrow the assignment to the two isomers predicted to be the lowest in energy at the MP2-F12/aug-cc-pVTZ-F12//MP2-aug-cc-pVDZ level of theory: isomer 1 and isomer 2. We experimentally assigned only *b*- and *c*-type transitions, with the *c*-type transitions being slightly more intense than the *b*-type transitions. This observation supports the identification of the observed Phe-$(H_2O)_3$ cluster as isomer 1 or 2, as they are the only isomers for which $\mu_c > \mu_b$ and a relatively weak μ_a are predicted by all computational methods employed in this work.

Table 2 Comparison between experimental and theoretical (MP2-F12/aug-cc-pVDZ-F12) spectroscopic constants for Phe-$(H_2O)_{n=1-3}$ complexes. The experimental rotational constants reported for the Phe-H_2O complex are an average of the rotational constants determined for the four tunnelling states.

	Phe-H_2O		Phe-$(H_2O)_2$		Phe-$(H_2O)_3$	
	Calc.	Exp.	Calc.	Exp.	Calc.	Exp.
A (MHz)	1077.0	1046.790(13)[a]	637.6	608.34055(28)	648.1	589.69684(31)
B (MHz)	447.1	439.70295(56)	485.1	488.36362(13)	383.5	397.04936(21)
C (MHz)	389.4	393.331(13)	314.8	310.79554(15)	336.9	322.57479(51)
Δ_J (kHz)	-	1.759(34)	-	0.02422(82)	-	0.0358(16)
Δ_{JK} (kHz)	-	4.112(35)	-	-0.2972 (66)	-	-0.9479(87)
Δ_K (kHz)	-	0.71475(34)	-	0.1409(93)	-	0.802(10)
δ_j (kHz)	-	1.6438(35)	-	-	-	-
δ_k (kHz)	-	-0.1638(15)	-	-0.0749(39)	-	-0.334(13)
P_a (uÅ)	979.5	975.722(21)	927.3	915.08669(46)	1019.1	991.2626(13)
P_b (uÅ)	318.4	308.147(21)	678.1	710.99522(46)	481.0	575.4408(13)
P_c (uÅ)	150.9	173.642(21)	114.5	119.75494(46)	298.8	281.5742(13)

$\|\mu_a\|/\|\mu_b\|/\|\mu_c\|$ (D)[b]	1.0/0.1/2.2	y/n/y	0.1/1.1/0.5	n/y/y	0.5/0.9/1.7	n/y/y
# lines fitted[c]	-	405	-	122	-	83
σ (kHz)[d]	-	12.5	-	5.5	-	4.5

[a] Standard error in parentheses in the unit of the last digit.

[b] Yes (y) or no (n) observation of *a*-, *b*-, and *c*-type transitions.

[c] Number of rotational transitions fitted.

[d] Standard deviation of the fit.

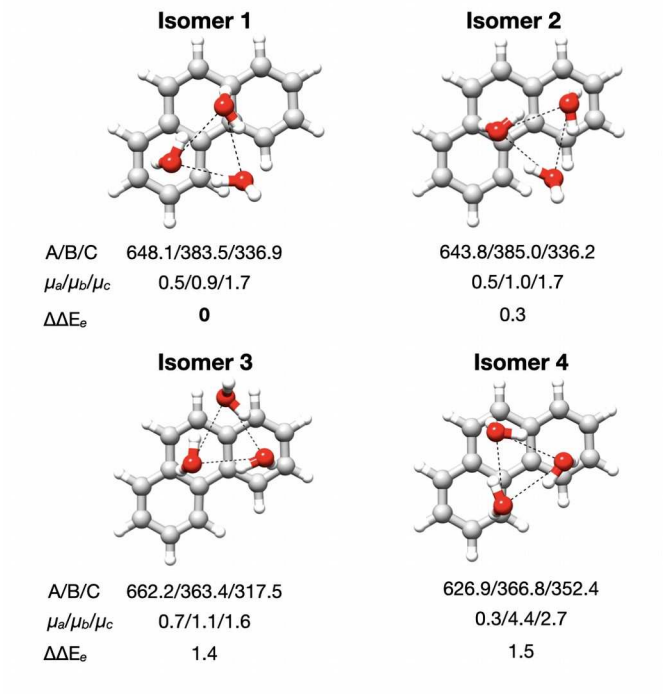

Figure 3 Theoretical structures calculated at the MP2/aug-cc-pVDZ level of theory of the four lowest energy isomers of the Phe-$(H_2O)_3$ exhibiting a clockwise directionality of the hydrogen bond network. The rotational constants (in MHz) and the absolute values of the principal dipole moment components (in Debye) calculated at the MP2/aug-cc-pVDZ level of theory are reported. Single point MP2-F12/aug-cc-pVTZ-F12//MP2/aug-cc-pVDZ relative energies ($\Delta\Delta E_e$) are also provided.

We performed NEB calculations at the B3LYP-D3BJ/def2-TZVP level of theory to calculate the interconversion barrier between the two isomers (Figure S18). As expected, this motion is essentially barrierless. This structural flexibility associated with low barriers is a further indication of the high mobility of water on the Phe surface, as already discussed in the case of Phe-H_2O. We can thus only conclude that the Phe-$(H_2O)_3$ complex identified in the experimental rotational spectrum could be either isomers 1 or 2, or an averaged structure of the two isomers. In this situation, the experimental structure of the observed Phe-$(H_2O)_3$ cluster could only be unambiguously identified using data from isotopic species, which is not available for the Phe-$(H_2O)_3$ cluster due to the rather low intensity of this species in the rotational spectrum.

The *ab initio* structure of the Phe-$(H_2O)_3$ complex reported in Figure 4 corresponds to isomer 1. For simplicity, we will be referring to this isomer in the following discussion. Nevertheless, considering the subtle geometrical differences between the two isomers, all the considerations reported below should also apply to isomer 2.

We have seen that the stepwise addition of a third water molecule brings about the observation of a cyclic water trimer sitting over the Phe aromatic cloud. The water trimer is similar to that observed in the Ace-$(H_2O)_3$ complex;[5] however, there are several differences as the water motif seen in Phe-$(H_2O)_2$ is preserved. The addition of the third water molecule moves W2 from sitting directly over the bay region to interacting with one of Phe's lateral rings, while W1's interaction with the hydrogen atoms in the bay region of Phe is preserved, albeit weaker, and contributes to the interaction network at play. A coaction between O–H···π and C–H···O interactions anchors the water trimer to the Phe molecule and stabilises the overall cluster. To account for the weak interaction with the bay hydrogen atoms, the cyclic water trimer resides on a plane tilted by approximately 9° with respect to the Phe surface. This quasi-parallel arrangement is reflected in the perpendicular distances between O1, O2, and O3 atoms and the Phe plane, calculated to be 2.67 Å, 3.11 Å, and 3.13 Å, respectively. This is in contrast to the structure of the Ace-$(H_2O)_3$ complex, in which the water cluster assumes an almost perfect parallel arrangement with respect to Ace, with the three water molecules sitting 3.25 Å, 3.29 Å, and 3.24 Å above the Ace surface.

Analogies between the Phe-$(H_2O)_3$ and Ace-$(H_2O)_3$ complexes are observed when comparing the water O···O distances between the two clusters and those of the bare water trimer. The theoretical O···O distances predicted for the Phe-$(H_2O)_3$ (O1–O2 = 2.79 Å, O2–O3 = 2.82 Å and O1–O3 = 2.88 Å) display clear similarities to the one calculated for the Ace-$(H_2O)_3$ complex (O1···O2 = 2.79 Å, O2···O3 = 2.77 Å and O1···O3 = 2.89 Å), in that in both complexes the water trimer assumes a distorted geometry with respect to the isolated cyclic water trimer.[48] The latter is known to exhibit a symmetric geometry in which the water monomers are equidistant (2.85 Å) from each other. These rearrangements within the water cluster in the Phe-$(H_2O)_3$ and Ace-$(H_2O)_3$ complexes are likely to be

caused by the interaction with the substrate. However, considering the irregularity observed between the *ab initio* and the experimental geometries of the Phe-$(H_2O)_2$ and Ace-$(H_2O)_2$ complexes, we cannot ensure that the reported *ab initio* values reflect the actual experimental structure.

Structural comparison between Pan-$(H_2O)_{n=1-3}$ and Phe-$(H_2O)_{n=1-3}$ clusters.

A comparison between the geometries of the Phe-$(H_2O)_{n=1-3}$ and Pan-$(H_2O)_{n=1-3}$ clusters reveals the effect of the nitrogen atom in the backbone of Pan on the interaction network and the geometry of the water cluster. On the one hand, the planarity of Phe and the absence of a preferred interaction site, such as the nitrogen atom in the backbone of Pan or the two out-of-plane hydrogen atoms in the case of Ace, lead to various binding motifs depending on the degree of hydration. On the other hand, the nitrogen atom in the skeleton of Pan constrains the water molecules to a specific interaction site so that an overall planar geometry with a linear chain of water molecules is preserved in spite of the degree of solvation.

The water binding motifs in the Phe-H_2O and Pan-H_2O clusters are unsurprisingly different. The different stability of the two clusters is reflected by the O···PAH distance of 3.359(4) Å and 2.926 (1) Å, in the Phe-H_2O and Pan-H_2O clusters, respectively. In the Phe-H_2O cluster, the overall complex is stabilised by weak intermolecular forces, which in combination with the symmetry of the molecule give rise to the observed internal dynamics. In the Pan-H_2O cluster, the interplay between the stronger O–H···N and C–H···O interactions locks the water molecule to a specific site and prevents any possible large amplitude motions. These interactions can be visualized in the NCI plots (Figure 4), which reveal the dominance of the weaker O–H···π interactions in the Phe-H_2O cluster and the stronger hydrogen bonds in Pan-H_2O.

Similarly to the monohydrated clusters, the structures of Phe-$(H_2O)_2$ and Pan-$(H_2O)_2$ show clear variations. The observed conformer of Phe-$(H_2O)_2$ exhibits a π bonded cluster, in which W1 interacts with both hydrogen atoms in the bay region and W2 forms O–H···π interactions with the aromatic π-cloud of phenanthrene. In contrast, interactions with the aromatic system are not observed in the Pan-$(H_2O)_2$ complex. The nitrogen atom in the skeleton of Pan decreases the electron density at the aromatic hydrogen atoms and makes them a more competitive interaction site for the water molecules. These dissimilarities result in a difference between the O···O distance of the two complexes. In Pan-$(H_2O)_2$, we see an O···O distance of 2.85(1) Å and for the Phe-$(H_2O)_2$ complex, an O···O distance of 2.793(3) Å is observed.

For the Phe-$(H_2O)_3$ complex, a cyclic motif of the water trimer is preferred over a linear one while the opposite is observed in the Pan-$(H_2O)_3$ cluster. In the case of Phe, the interaction between the water trimer and the aromatic π electron system of Phe is predominantly dispersive. In such a system, the water-water interactions are stronger and more competitive than the water-π interactions. Also, a cyclic arrangement of the water molecules maximizes the number of hydrogen bond interactions, thereby increasing the stability of the cluster.

In the Pan-$(H_2O)_3$ complex, the preferred linear motif of the water cluster can also be rationalised in terms of number of interactions established with the PAH. In Pan this value is greater when the water molecules assume a linear motif compared to the cyclic arrangement. Furthermore, as mentioned before, the inductive effect (I^-) of the nitrogen atom reduces the electron density at the adjacent hydrogen atoms making them a preferred site of interactions for the water molecules. A comparison between the *ab initio* values of the O···O distances in the two complexes also highlights the influence that the nitrogen atom has on the strength of the water-water interactions. Indeed, for the Pan-$(H_2O)_3$, the O···O distances have been calculated to be 0.1 Å shorter than those predicted for the Phe-$(H_2O)_3$ complex (Figure 4).

Intermolecular interactions in the Pan-$(H_2O)_{n=1-3}$ and Phe-$(H_2O)_{n=1-3}$ clusters.

Size, shape, and degree of aromaticity of a PAH influence the strength of the interactions established within the PAH-water complex and thereby the overall stability of the cluster**.** An informative picture of this can be obtained from a Symmetry Adapted Perturbation Theory (SAPT) [49] analysis, known for its ability to decompose the total interaction energy into its different contributions: electrostatics, dispersion, induction, and exchange. As previously mentioned, this method is generally applied to two-body molecular systems or to larger clusters that can be treated as a two-body system. This is not the case for the higher order clusters of Pan (> one water molecule), where strong hydrogen bonds play the major role. Therefore, an SAPT analysis was only carried out on the Pan-H_2O and Phe-$(H_2O)_{n=1-3}$ complexes. The obtained results have then been compared with those of related systems, such as the water dimer, benzene-water,[44,45] and the Ace-water complexes[5], and are showcased in Table 3. The percent contribution of each attractive component (electrostatics, induction, and dispersion) to the total attractive interaction energy is illustrated in a bar chart in Figure 8 for all systems taken into consideration.

Table 3 Interaction energies (kJ mol^{-1}) calculated at the SAPT2+3/aug-cc-pVDZ level of theory.

	ΔE_{Elst}	ΔE_{Ind}	ΔE_{Disp}	ΔE_{Exch}	ΔE_{Tot}
$(H_2O)_2$	-34.2	-10.4	-9.5	35.0	-19.1
Pan-H_2O	-56.5	-21.8	-21.8	69.0	-30.5
Benzene-H_2O	-13.3	-5.5	-14.5	21.3	-12.1
Ace-H_2O	-21.6	-6.1	-23.0	32.9	-17.9
Phe-H_2O	-14.8	-5.0	-18.6	24.6	-13.8
Ace-$(H_2O)_2$	-36.9	-15.4	-38.4	54.8	-35.9

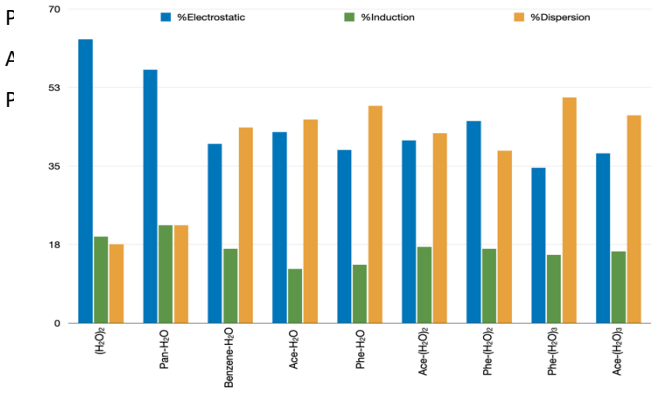

Figure 8 Bar chart showing the attractive components (electrostatic, induction, and dispersion) for $(H_2O)_2$, benzene-H_2O, Pan-H_2O, Phe-$(H_2O)_{n=1-3}$, and Ace-$(H_2O)_{n=1-3}$ complexes as a percentage of the total attractive interaction energy ($\Delta E_{\chi o \mu \pi o \nu \varepsilon \nu t}/\Delta E_{\tau o \tau \alpha \lambda}$).

The monohydrated clusters of Pan and Phe have different interaction energy profiles. In the Pan-H_2O complex, the electrostatic component clearly dominates over the dispersion one, with the first accounting for 56% of the total attractive interaction energy and the latter accounting for only 22%. The Phe-H_2O is more stabilised by an interplay between electrostatic (39%) and dispersion (48%) interactions. A similar competition between the electrostatic and dispersion contribution also characterises the interaction energy profile of the higher order water clusters of Phe.

As electrostatics is the dominant interaction stabilising the Pan-H_2O cluster, this system is more similar to the water dimer than all the other systems considered here. Clear similarities are observed between Phe-H_2O, Ace-H_2O, and benzene-H_2O complexes, in that they display an interplay between dispersive and electrostatic interactions. The dispersion component is greater than the electrostatic and inductive components, accounting for about 48%, 45%, and 44% of the total attractive interaction energy. The interaction energy profile of Phe-$(H_2O)_2$ can be compared with the one of the Ace-$(H_2O)_2$ complex. As shown in the bar chart reported in Figure 8, in the Phe-$(H_2O)_2$, the electrostatic interaction component (45%) slightly dominates over the dispersion one (38%), whereas in the Ace-$(H_2O)_2$ complex, dispersion and electrostatic energies are found to contribute almost equally to the stability of the complex (41% and 42%, respectively). This is in line with the differences observed in the experimental geometries of the two complexes. The aromatic hydrogen atoms in the bay region of Phe create a stronger C-H···O interaction with W1 than the aliphatic out-of-plane hydrogen atoms in Ace, resulting in the shorter O···O distance in Phe-$(H_2O)_2$ compared to Ace-$(H_2O)_2$. The interaction energy profile of the Phe-water complexes is reversed upon addition of a third water molecule with the dispersion interaction component now being predominant and accounting for 46% and the electrostatic component accounting for 35% of the total attractive interaction energy. These values hint towards the fact that the Phe-$(H_2O)_3$ complex is similar to the Ace-$(H_2O)_3$ complex and in turn towards similar O···O distances in the experimental structure.

The fact that the ratio between the interaction energy components changes with the stepwise addition of water molecules onto the Phe surface reflects the structural differences observed between the Phe-$(H_2O)_{n=1-3}$ complexes. The differences observed between the Phe-$(H_2O)_{n=1-3}$ and Ace-$(H_2O)_{n=1-3}$ further confirm that the topology of the PAHs influences the nature of the interaction energy profile of the cluster.

Conclusions

Phe and Pan have been successfully complexed with up to three water molecules, and their structures have been investigated by means of high-resolution broadband rotational spectroscopy in combination with quantum chemical calculations. Despite the structural similarities between the two molecules, the presence of a heteroatom in the backbone of Pan dramatically changes the potential energy landscape, with in-plane growth geometries of the Pan-water clusters preferred over the out-of-plane growth geometries observed for the Phe-water clusters.

We have seen that the planarity of Phe and the lack of a preferred site of interaction allow for a remarkable mobility of the water in its monohydrated complex. This leads to a significant rearrangement of the geometry of the cluster upon addition of water molecules, always favouring the interaction with the bay region of the PAH. In the Pan-water complexes, the strong O–H···N interaction locks the water molecule to the nitrogen atom, thereby preserving the overall planar geometry of the cluster with increasing degree of hydration.

Based on our findings, we hypothesize that the composition of the PAH influences the local morphology of interstellar ice build-up in space and thus potentially impacts the chemical processes occurring in these environments. For example, we have shown here that the hydrogen atoms in the bay region of Phe are the water's preferred interaction sites in the Phe-water complexes, whereas the nitrogen atom in the backbone of Pan directs the water interaction to the hydrogen atoms adjacent to the nitrogen. Therefore, one could speculate that different ice morphologies could favour different sites for hydrogen loss or hydrogen addition, thus impacting chemical processes. One example could be the UV photolysis of PAHs in the presence of water molecules, which could lead to the formation of oxygenated PAHs.

In a more general context, the results provided here can be used to improve and advance the ability of modelling aromatic-polar interactions involving aromatic substrates of different nature in a diverse range of chemical and biological processes.

Conflicts of interest

There are no conflicts to declare.

Acknowledgements

This work has been supported by the ERC Starting grant 'Astrorot' (grant agreement number 638027). D.L and P.P acknowledge the support of Alexander von Humboldt postdoctoral fellowships. A.M.R acknowledges support via a Mildred-Dresselhaus guest professorship.

Notes and references

1 E. A. Meyer, R. K. Castellano and F. Diederich, *Angewandte Chemie International Edition*, 2003, **42**, 1210–1250.
2 C. Joblin and G. Mulas, *EAS Publications Series*, 2009, **35**, 133–152.
3 M. P. Bernstein, S. A. Sandford, L. J. Allamandola, J. S. Gillette, S. J. Clemett and R. N. Zare, *Science*, 1999, **283**, 1135–1138.
4 Z. Guennoun, C. Aupetit and J. Mascetti, *J. Phys. Chem. A*, 2011, **115**, 1844–1852.
5 A. L. Steber, C. Pérez, B. Temelso, G. C. Shields, A. M. Rijs, B. H. Pate, Z. Kisiel and M. Schnell, *J. Phys. Chem. Lett.*, 2017, **8**, 5744–5750.
6 A. K. Lemmens, S. Gruet, A. L. Steber, J. Antony, S. Grimme, M. Schnell and A. M. Rijs, *Phys. Chem. Chem. Phys.*, 2019, **21**, 3414–3422.
7 S. R. Domingos, K. Martin, N. Avarvari and M. Schnell, *Angewandte Chemie International Edition*, 2019, **58**, 11257–11261.
8 C. Pérez, A. L. Steber, A. M. Rijs, B. Temelso, G. C. Shields, J. C. Lopez, Z. Kisiel and M. Schnell, *Phys. Chem. Chem. Phys.*, 2017, **19**, 14214–14223.
9 K. Chatterjee and O. Dopfer, *Chem. Sci.*, 2018, **9**, 2301–2318.
10 D. Schmitz, V. Alvin Shubert, T. Betz and M. Schnell, *Journal of Molecular Spectroscopy*, 2012, **280**, 77–84.
11 C. Pérez, A. Krin, A. L. Steber, J. C. López, Z. Kisiel and M. Schnell, *J. Phys. Chem. Lett.*, 2016, **7**, 154–160.
12 C. M. Western, *Journal of Quantitative Spectroscopy and Radiative Transfer*, 2017, **186**, 221–242.
13 H. M. Pickett, *Journal of Molecular Spectroscopy*, 1991, **148**, 371–377.
14 PROSPE - Programs for ROtational SPEctroscopy, http://www.ifpan.edu.pl/~kisiel/prospe_test.htm, (accessed 30 September 2020).
15 Chr. Møller and M. S. Plesset, *Phys. Rev.*, 1934, **46**, 618–622.
16 T. H. Dunning, *The Journal of Chemical Physics*, 1989, **90**, 1007–1023.
17 D. E. Goldberg, *Genetic Algorithms in Search, Optimization and Machine Learning*, Addison-Wesley Longman Publishing Co., Inc., USA, 1st edn., 1989.
18 J. M. Dieterich and B. Hartke, *Molecular Physics*, 2010, **108**, 279–291.
19 J. J. P. Stewart, *J Mol Model*, 2013, **19**, 1–32.
20 R. Sure and S. Grimme, *Journal of Computational Chemistry*, 2013, **34**, 1672–1685.
21 James J. P. Stewart, *MOPAC 2009 Computational Chemistry*, 2008. https://OpenMOPAC.net (2008)
22 F. Neese, *WIREs Computational Molecular Science*, 2012, **2**, 73–78.
23 F. Neese, *WIREs Computational Molecular Science*, 2018, **8**, e1327.
24 S. Grimme, S. Ehrlich and L. Goerigk, *Journal of Computational Chemistry*, 2011, **32**, 1456–1465.
25 F. Weigend and R. Ahlrichs, *Phys. Chem. Chem. Phys.*, 2005, **7**, 3297–3305.
26 R. M. Parrish, L. A. Burns, D. G. A. Smith, A. C. Simmonett, A. E. DePrince, E. G. Hohenstein, U. Bozkaya, A. Yu. Sokolov, R. Di Remigio, R. M. Richard, J. F. Gonthier, A. M. James, H. R. McAlexander, A. Kumar, M. Saitow, X. Wang, B. P. Pritchard, P. Verma, H. F. Schaefer, K. Patkowski, R. A. King, E. F. Valeev, F. A. Evangelista, J. M. Turney, T. D. Crawford and C. D. Sherrill, *J. Chem. Theory Comput.*, 2017, **13**, 3185–3197.
27 E. R. Johnson, S. Keinan, P. Mori-Sánchez, J. Contreras-García, A. J. Cohen and W. Yang, *J. Am. Chem. Soc.*, 2010, **132**, 6498–6506.
28 T. Lu and F. Chen, *Journal of Computational Chemistry*, 2012, **33**, 580–592.
29 A. E. Reed, R. B. Weinstock and F. Weinhold, *J. Chem. Phys.*, 1985, **83**, 735–746.
30 G. Henkelman, B. P. Uberuaga and H. Jónsson, *J. Chem. Phys.*, 2000, **113**, 9901–9904.
31 D. McNaughton, P. D. Godfrey, R. D. Brown and S. Thorwirth, *Phys. Chem. Chem. Phys.*, 2007, **9**, 591–595.
32 D. McNaughton, P. D. Godfrey, R. D. Brown, S. Thorwirth and J.-U. Grabow, *ApJ*, 2008, **678**, 309.
33 J. Kraitchman, *American Journal of Physics*, 1953, **21**, 17–24.
34 J. K. G. Watson, A. Roytburg and W. Ulrich, *Journal of Molecular Spectroscopy*, 1999, **196**, 102–119.
35 Z. Kisiel, *Journal of Molecular Spectroscopy*, 2003, **218**, 58–67.
36 P. Matczak and S. Wojtulewski, *J Mol Model*, 2015, **21**, 41.
37 G. A. Jeffrey, *An Introduction to Hydrogen Bonding*, Oxford University Press, 1997.
38 P. Gilli, V. Bertolasi, V. Ferretti and G. Gilli, *J. Am. Chem. Soc.*, 2000, **122**, 10405–10417.
39 S. Blanco, P. Pinacho and J. C. López, *Angewandte Chemie International Edition*, 2016, **55**, 9331–9335.
40 S. Gruet, C. Pérez, A. L. Steber and M. Schnell, *Phys. Chem. Chem. Phys.*, 2018, **20**, 5545–5552.
41 J. C. López, R. Sánchez, S. Blanco and J. L. Alonso, *Phys. Chem. Chem. Phys.*, 2014, **17**, 2054–2066.
42 P. Pinacho, J. C. López, Z. Kisiel and S. Blanco, *Phys. Chem. Chem. Phys.*, 2020, **22**, 18351–18360.
43 P. Pinacho, D. A. Obenchain and M. Schnell, *The Journal of Chemical Physics*, 2020, **153**, 234307.
44 S. Suzuki, P. G. Green, R. E. Bumgarner, S. Dasgupta, W. A. Goddard and G. A. Blake, *Science*, 1992, **257**, 942–945.
45 H. S. Gutowsky, T. Emilsson and E. Arunan, *J. Chem. Phys.*, 1993, **99**, 4883–4893.
46 E. M. Cabaleiro-Lago, J. Rodríguez-Otero and Á. Peña-Gallego, *J. Phys. Chem. A*, 2008, **112**, 6344–6350.
47 T. R. Dyke and J. S. Muenter, *J. Chem. Phys.*, 1974, **60**, 2929–2930.
48 F. N. Keutsch and R. J. Saykally, *PNAS*, 2001, **98**, 10533–10540.
49 K. Szalewicz, *WIREs Computational Molecular Science*, 2012, **2**, 254–272.

